Site Connectivities in Amorphous Materials Studied by Double-Resonance NMR of Quadrupolar Nuclei: High-Resolution $^{11}B \leftrightarrow {}^{27}Al$ Spectroscopy of Aluminoborate Glasses

Jerry C. C. Chan, Marko Bertmer, and Hellmut Eckert*

Contribution from the Institut für Physikalische Chemie, Westfälische Wilhelms-Universität Münster, Schlossplatz 7, D-48149 Münster, Germany

Abstract: The utility of heteronuclear double-resonance NMR methods involving the quadrupolar nuclei ^{11}B and ^{27}Al is demonstrated for probing the *intermediate-range order* in aluminoborate glasses. Results from both rotational echo double resonance (REDOR) and heteronuclear cross-polarization magic angle spinning (CPMAS) studies are presented and discussed. While both techniques are strongly affected by the presence of large quadrupolar splittings, a working strategy is developed on the basis of which reliable structural interpretations are possible. Using this strategy, the effects of the cation type M on the structures of two basic glass compositions, $25M_{(2)}O\text{-}45B_2O_3\text{-}30Al_2O_3$ and $40M_{(2)}O\text{-}40B_2O_3\text{-}20Al_2O_3$ (M = Na, Ca, Mg), are discussed. Within each series having the same basic network composition, replacement of the modifier cation Na by Ca or Mg produces a large change in the speciation of framework aluminum ("cation effect"): while in the sodium-containing glass the overwhelming fraction of Al is present as tetrahedral $AlO_{4/2}$ sites, the calcium- and magnesium-containing glasses also possess larger fractions of five- and six-coordinated aluminum sites. $^{27}Al\{^{11}B\}$ REDOR results indicate that all of these aluminum environments interact equally strongly with the dominant $BO_{3/2}$ sites in both glasses. In addition, the reverse $^{11}B\{^{27}Al\}$ REDOR results reveal that the extent of the $AlO_{4/2}-BO_{4/2}$ interaction in the network is highly dependent on the framework composition and on the M cation type. While sodium aluminoborate glasses reveal strong chemical ordering (avoidance of intertetrahedral linkages), the analogous Mg^{2+}-based glasses tend toward a randomization of connectivities. Finally, two-dimensional heteronuclear correlation spectra obtained via $^{11}B\{^{27}Al\}$ CPMAS suggest that AlO_5 and AlO_6 sites can provide a mechanism for stabilizing tetrahedral $BO_{4/2}$ units.

Introduction

High-resolution solid-state NMR spectroscopy has become an indispensable method in the structural analysis of amorphous systems and glasses.[1,2] In particular, using the technique of magic angle spinning (MAS), it has been possible to identify and quantify the nearest-neighbor atomic environments, which constitute the *short-range order* of these materials. When nuclei with large nuclear electric quadrupolar interactions are involved, the resolution of MAS can be further improved by focusing the attention on satellite transitions (SATRAS)[3−7] or by using multiple-quantum excitation (MQMAS) NMR.[8−10] While these methods thence allow the glass to be quantitatively described in terms of individual structural units, they give no information on the question of how these units are linked in forming the overall network. Such "site connectivities", spatial proximities,

and other ordering/disordering phenomena occurring on larger length scales (*intermediate-range order*) have become an important scientific issue in current glass research.[11] The most informative NMR parameter in this respect is the magnetic dipole−dipole coupling, because it is rigorously dependent on internuclear distances and distributions thereof.[12] These dipolar couplings cannot be measured in simple MAS experiments, because MAS is specifically designed to eliminate all anisotropic interactions (chemical shift anisotropy, dipolar interaction, etc.) affecting solid-state NMR spectra.[13] In recent years, however, advanced double-resonance techniques have been developed, which selectively reintroduce these dipolar couplings and thereby allow their measurement under high-resolution solid-state NMR conditions. Experiments of this type include cross-polarization/magic angle spinning (CPMAS),[14] rotational echo double resonance (REDOR),[15,16] transferred echo double resonance,[17] heteronuclear double-quantum spectroscopy,[18] and other

(1) Eckert, H. *Prog. NMR Spectrosc*. **1992**, *24*, 159.
(2) Eckert, H. *NMR: Basic Princ. Prog.* **1994**, *33*, 125.
(3) Samoson, A. *Chem. Phys. Lett*. **1985**, *119*, 29.
(4) Lippmaa, E.; Samoson, A.; Mägi, M. *J. Am. Chem. Soc*. **1986**, *108*, 1730.
(5) Jakobsen, H. J.; Skibsted, J.; Bildsøe, H.; Nielsen, N. C. *J. Magn. Reson*. **1989**, *85*, 173.
(6) Jäger, C.; Müller-Warmuth, W.; Mundus, C.; van Wüllen, L. *J. Noncryst. Solids* **1992**, *149*, 209.
(7) Jäger, C. *NMR: Basic Princ. Prog.* **1994**, *31*, 134.
(8) Medek, A.; Harwood, J. S.; Frydman, L. *J. Am. Chem. Soc.* **1995**, *117*, 12779.
(9) Fernandez, C.; Amoureux, J. P. *Chem. Phys. Lett*. **1995**, *242*, 449.
(10) Fernandez, C.; Amoureux, J. P. *Solid State Nucl. Magn. Reson.* **1996**, *5*, 315.

(11) Elliot, S. R. *Nature (London)* **1991**, *354*, 445.
(12) van Vleck, J. H. *Phys. Rev*. **1948**, *54*, 1168.
(13) Mehring, M. *Principles of High-Resolution NMR in Solids*; Springer-Verlag: Berlin, 1983.
(14) Stejskal, E. O.; Schaefer, J. *J. Magn. Reson*. **1975**, *18*, 560.
(15) Gullion, T.; Schaefer, J. *J. Magn. Reson*. **1989**, *81*, 196.
(16) Garbow, J. R.; Gullion, T. *J. Magn. Reson*. **1991**, *95*, 442.
(17) Hing, A. W.; Vega, S.; Schaefer, J. *J. Magn. Reson A* **1993**, *103*, 151.
(18) Saalwächter, K.; Graf, R.; Demco, D. E.; Spiess, H. W. In *Proceedings of the Joint 29th AMPERE−13th ISMAR International Conference*; Ziessow, D., Lubitz, W., Lendzian, F., Eds.; Technische Universität Berlin: Berlin, 1998; Vol. I, p 294.

methods.[19,20] A variety of intriguing applications to inorganic materials, glasses, and ceramics have appeared in the literature.[21-32] For example, interactions between guest molecules and atoms in the host framework of zeolites have been studied, including the detailed quantification of internuclear distances.[29,31] Other studies have successfully applied CPMAS or REDOR to demonstrate connectivities in a variety of glasses[25-28] and crystalline model compounds.[21-24]

The present study concerns the structure of aluminoborate glasses $(M_{(2)}O)_y$-$(B_2O_3)_x$-$(Al_2O_3)_{1-x-y}$, where M is an alkali or alkaline-earth metal. These glasses are useful for a variety of industrial applications.[33,34] A microscopic understanding of their structures facilitates the tailoring of their physical and chemical properties to specifically desired applications.[35,36] Regular MAS NMR studies have shown the presence of two boron sites, trigonal $BO_{3/2}$ units and tetrahedral $BO_{4/2}$ sites, while aluminum can occur in four-, five-, and six-coordination.[37-43] As in any other glass system, the quantitative proportions of these units depend on the elemental composition. In addition, it is well-known that the nature of the M cation exercises a great influence in determining the relative proportions of the structural speciation.[44] To gain a more fundamental understanding of this "cation effect", we explore preferential connectivities among the boron and aluminum sites using both CPMAS and REDOR experiments involving the nuclei ^{11}B (spin $^3/_2$) and ^{27}Al (spin $^5/_2$). To focus specifically on the cation effect, two compositional series were selected (glasses I and II), within which the cation type M is changed from Na to Ca to Mg (accordingly, the sample notations are Mg-I, Ca-I, Na-I; Mg-II, Ca-II, Na-II).

(19) Grey, C. P.; Veeman, W. S.; Vega, A. J. *J. Chem. Phys.* **1993**, *98*, 7711.

(20) Gullion, T. *Chem. Phys. Lett.* **1995**, *246*, 325.

(21) Fyfe, C. A.; Grondey, H.; Mueller, K. T.; Wong-Moon, K. C.; Markus, T. *J. Am. Chem. Soc.* **1992**, *114*, 5876.

(22) Fyfe, C. A.; Mueller, K. T.; Grondey, H.; Wong-Moon, K. C. *J. Phys. Chem.* **1993**, *97*, 13484.

(23) Fyfe, C. A.; Wong-Moon, K. C.; Grondey, H.; Mueller, K. T. *J. Phys. Chem.* **1994**, *98*, 2139.

(24) Fyfe, C. A.; Wong-Moon, K. C.; Huang, Y.; Grondey, H.; Mueller, K. T. *J. Phys. Chem.* **1995**, *99*, 9, 8707.

(25) De Paul, S. M.; Ernst, M.; Shore, J. S.; Stebbins, J. F.; Pines, A. *J. Phys. Chem. B* **1997**, *101,* 3240.

(26) Van Wüllen, L.; Züchner, L.; Müller-Warmuth, W.; Eckert, H. *Solid State Nucl. Magn. Reson.* **1996**, *6*, 203.

(27) van Wüllen, L.; Gee, B.; Züchner, L.; Bertmer, M.; Eckert, H. *Ber. Bunsen-Ges. Phys. Chem.* **1996**, *100*, 1539.

(28) Herzog, K.; Thomas, B.; Sprenger, D.; Jäger, C. *J. Noncryst. Solids* **1995**, *190*, 296.

(29) Fyfe, C. A.; Lewis, A. R.; Chezeau, J. M.; Grondey, H. *J. Am. Chem. Soc.* **1997**, *119*, 12210.

(30) Holl, S. M.; Kowalewski, T.; Schaefer, J. *Solid State Nucl. Magn. Reson.* **1996**, *6*, 39.

(31) Grey, C. P.; Arun Kumar, B. S. *J. Am. Chem. Soc.* **1995**, *117*, 9071.

(32) Blumenfeld, A. L.; Coster, D.; Fripiat, J. J. *J. Phys. Chem.* **1995**, *99*, 15181.

(33) DeWaal, H. *Phys. Chem. Glasses* **1962**, *3*, 1.

(34) Owen, A. E. *Phys. Chem. Glasses* **1961**, *2*, 87, 152.

(35) Tuller, H. J.; Button, D. P.; Uhlmann, D. R. *J. Noncryst. Solids* **1980**, *40*, 93.

(36) Gough, E.; Isard, J. O.; Topping, J. A. *Phys. Chem. Glasses* **1969**, *10*, 89.

(37) Gresch, R.; Müller-Warmuth, W.; Dutz, H. *J. Noncryst. Solids* **1976**, *21*, 31.

(38) Zhong, J.; Bray, P. J. *J. Noncryst. Solids* **1986**, *84*, 17.

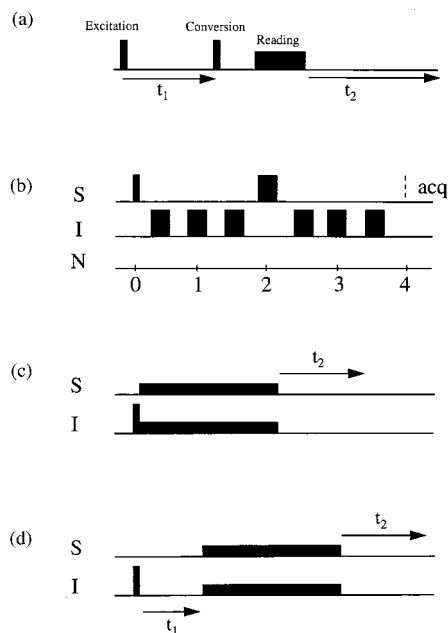(39) Dupree, R.; Holland, D.; Williams, D. S. *Phys. Chem. Glasses* **1985**, *26*, 50.

(40) Bunker, B. C.; Kirkpatrick, R. J.; Brow, R. K.; Turner, G. L.; Nelson, C. *J. Am. Ceram. Soc.* **1991**, *74*, 1430.

(41) Hähnert, M.; Hallas, E. *Rev. Chim. Miner.* **1987**, *24*, 221.

(42) Bunker, B. C.; Kirkpatrick, R. J.; Brow, R. K. *J. Am. Ceram. Soc.* **1991**, *74*, 1425.

(43) Züchner, L.; Chan, J. C. C.; Müller-Warmuth, W.; Eckert H. *J. Phys. Chem.* **1998**, *102*, 4495.

(44) Hallas, E.; Gerth, K.; Hähnert, M. *Z. Chem.* **1987**, *27*, 270.

Figure 1. Pulse sequences employed in this work. (a) *Z*-filtering TQMAS sequence; (b) REDOR; (c) double-quantum CPMAS; (d) CPMAS−HETCOR.

Applications of heteronuclear CPMAS and REDOR techniques to spin > $^1/_2$ nuclei experiencing strong electric quadrupolar interactions encounter severe complications. For example, the process of spin-locking, an essential part of the standard CP experiment, is severely compromised by spin transitions effected under continuous wave irradiation while spinning at the magic angle.[45,46] Similarly, large quadrupolar splittings affect REDOR studies, as the pulse trains applied in the course of these experiments may or may not affect only the populations of the central spin states.[47] Owing to these intrinsic difficulties, it is understandable why the literature is almost devoid of high-resolution double-resonance experiments in which both of the nuclear spin species involved are quadrupolar. Previous exceptions include our exploratory $^{11}B-^{27}Al$ double-resonance experiments on aluminoborate glasses,[26,48] which we are expanding upon in the present work. An important goal of this study is to outline a general experimental strategy for obtaining reliable structural information in systems containing two types of quadrupolar nuclei.

Principles and Methodology

High-Resolution NMR of Quadrupolar Nuclei. The pulse sequences used in this work are summarized in Figure 1. Part a shows the two-dimensional triple-quantum (TQ) NMR technique that is now commonly employed for recording high-resolution MAS NMR spectra of quadrupolar nuclei.[49] This technique exploits the fact that the $|^3/_2\rangle \leftrightarrow |-^3/_2\rangle$ triple-quantum transition, albeit forbidden, has no intrinsic anisotropy arising from the first-order quadrupolar coupling. The first pulse excites triple-quantum coherence, which is allowed to evolve for the duration of the evolution time, t_1. The evolution is then stopped by the second pulse. The third pulse (generally applied at a lower

(45) Vega, A. J. *J. Magn. Reson.* **1992**, *96*, 50.

(46) Vega, A. J. *Solid State Nucl. Magn. Reson.* **1992**, *1*, 17.

(47) Chopin, L.; Vega, S.; Gullion, T. *J. Am. Chem. Soc.* **1998**, *120*, 4406.

(48) Chan, J. C. C.; Bertmer, M.; Eckert H. *Chem. Phys. Lett.* **1998**, *292*, 154.

(49) Amoureux, J. P.; Fernandez, C.; Steuernagel, S. *J. Magn. Reson.* **1996**, *A123*, 116.

power level) produces single-quantum coherence, corresponding to observable magnetization. Incrementation of t_1 and subsequent 2-D data processing allows the regular MAS spectrum (dominated by second-order broadening) to be correlated with a spectrum that is solely governed by isotropic quadrupolar shifts and chemical shifts, δ_{iso}. In the present contribution, the TQMAS sequence is used to record high-resolution MAS NMR spectra of the ^{27}Al nuclei and to quantify their interaction parameters. Complementary results are obtained using SATRAS, which can provide quantitative estimates of the various aluminum species present, as previously shown.[7] High-resolution ^{11}B NMR spectra are obtained by the standard MAS approach. In this case, the principal component (C_Q) and the asymmetry parameter (η) of the nuclear electric quadrupolar interaction tensor as well as δ_{iso} are obtained by computer simulation using second-order perturbation theory.[50] The initial fitting parameters are taken from our previous work on sodium aluminoborate glasses.[43] In addition, values of $\chi = C_Q(1 + \eta^2/3)^{1/2}$ are listed.

REDOR NMR of Multiple-Spin Systems Involving Quadrupolar Nuclei. Figure 1b shows the REDOR pulse sequence used in the present study. This pulse sequence reintroduces the heteronuclear dipolar coupling that is normally averaged out by MAS into the high-resolution NMR experiment.[51] Basically, the magnetization of one spin species ("spin S") is observed by a rotor-synchronized spin–echo sequence while 180° pulses are being applied to the other spin species ("spin I") in the middle of each rotor period. These 180° pulses reverse the sign of the I–S dipole–dipole coupling constant, thereby preventing cancellation of this interaction by coherent averaging through MAS. As a consequence, the S spin–echo is attenuated. Thus the presence of a significant I–S dipole–dipole coupling can be substantiated by calculating the difference signal $\Delta S = S_o - S$ of two experiments executed in the absence and presence of the 180° (I) pulses. The magnitude of the (normalized) difference signal depends (a) on the I–S dipole–dipole coupling constant and (b) on the length of the evolution time during which the dipolar coupling is active. This time scale is under experimental control and given by NT_r, the number of rotor cycles (N) multiplied by the period of one rotor revolution (T_r). Thus, a plot of $\Delta S/S_o$ versus NT_r provides information about the strength of the dipolar coupling. For a two-spin system of spin $^1/_2$ nuclei, it has been derived that[15,16]

$$\frac{\Delta S}{S_0} = 1 - \frac{1}{2\pi}\int_0^\pi \int_0^\pi \cos(\Delta\Phi)\,\sin\beta\,d\alpha\,d\beta \qquad (1)$$

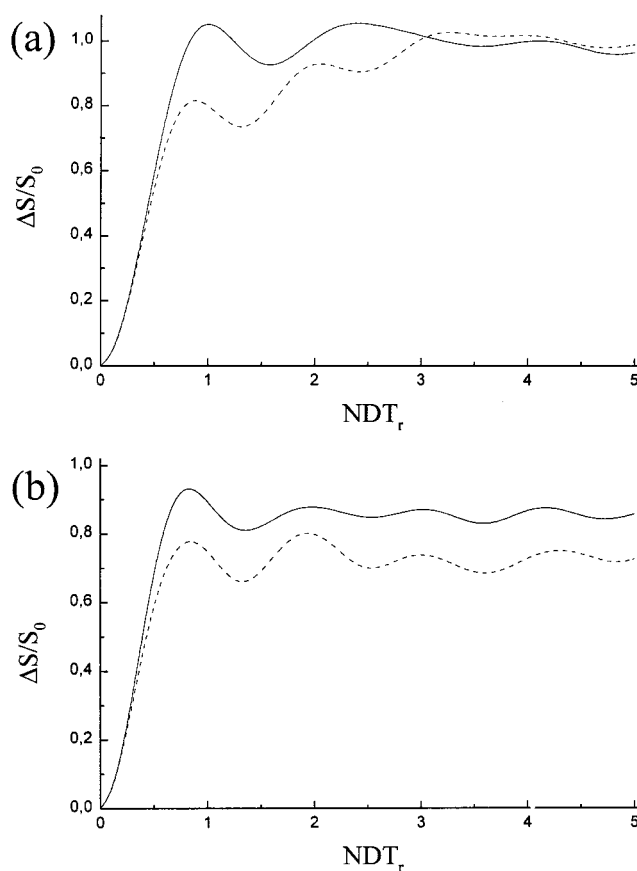where

$$\Delta\Phi = 2\sqrt{2}NT_rD\sin 2\beta \sin\alpha \qquad (2)$$

with

$$D = \frac{\mu_0}{4\pi}\frac{\gamma_I\gamma_S\hbar}{2\pi r^3} \qquad (3)$$

Here, α and β are the Euler angles relating the principal axis system to the laboratory coordinate system. Fitting the experimental REDOR curve to eq 1 then results in a dipole–dipole coupling constant D, from which the internuclear distance r can be calculated from eq 3. (Other symbols carry their usual meanings.)

Figure 2. Calculated REDOR dephasing curve of (a) an SI_3 system (solid line, trigonal plane; dashed line, trigonal pyramid) and (b) an SI_4 system (solid line, tetrahedral; dashed line, square planar).

The situation for aluminoborate glasses is more complicated, however, because these systems do not contain isolated spin pairs but have multiple I–I, S–S, and I–S interactions, where I and S denote the ^{11}B and the ^{27}Al nuclei, respectively, because of the interlinking of the boron and aluminum coordination polyhedra. The effects of such multiple-spin interactions on REDOR dephasing have been treated theoretically for systems only involving spin $^1/_2$ nuclei.[52,53] As shown by Naito et al.,[52] the shape of the REDOR dephasing curve of a three-spin system is sensitively dependent on the geometry of the system considered. Goetz and Schaefer have extended this approach to larger spin systems.[53] In particular, their simulations outline conditions under which the I–I homodipolar interaction does not affect the dephasing of S spins in a significant way; this is true in particular for the REDOR behavior at short evolution times, which will be the focus of the present study (see below). Figure 2 shows the results of simulations carried out in our own laboratory for a number of spin geometries, using the approach of Naito et al.[52] Following Gullion and Schaefer,[15] universal curves are displayed by plotting the normalized echo amplitude differences, $\Delta S/S_o$, as a function of DNT_r. Figure 2a illustrates the dephasing of S spin–echo intensity due to the coupling to three heteronuclei (I) in trigonal planar and trigonal pyramidal coordination geometries ("SI_3 systems"). Figure 2b shows corresponding plots for square planar and tetrahedral environments in SI_4 systems. These particular spin geometries were chosen for the simulations as they may be present in our glasses, where three- and four-coordinated units are interlinked by

(50) Samoson, A.; Kundla, E.; Lippmaa, E. *J. Magn. Reson.* **1982**, *49*, 350.
(51) Gullion, T. *Magn. Reson. Rev.* **1997**, *17*, 83.

(52) Naito, A.; Nishimura, K.; Tuzi, S.; Saitô, H. *Chem. Phys. Lett* **1994**, *229*, 506.
(53) Goetz, J. M.; Schaefer, J. *J. Magn. Reson.* **1997**, *117*, 1247.

oxygen. While the comparison of the dashed and solid curves in both parts a and b of Figure 2 reveals that the dephasing curves are highly dependent on the geometry of the spin system considered, these curves do converge at short evolution times, where the relative dephasing $\Delta S/S_o$ does not exceed the limiting value of 0.2. Thus, these simulations show that, for a given order of a spin system, the geometry dependence of the dephasing curves is negligible in the limit of short dipolar evolution times. In this limit, the REDOR dephasing curves can be approximated by a simple analytical function:[15]

$$\frac{\Delta S}{S_o} = \frac{16}{15}(NT_r)^2[D_1^2 + D_2^2 + ... + D_n^2] \quad (4a)$$

where $\sum D_i^2$ can be related to the dipolar second moment, M_2^{IS}, resulting in the expression

$$\frac{\Delta S}{S_0} = \frac{4}{3\pi^2}(NT_r)^2 M_2^{IS} \quad (4b)$$

Equation 4 allows the dipolar coupling to be quantified in spin systems of unknown order and geometry.[54] As an important feature of REDOR, site-selective heterodipolar second moments are obtained due to the high resolution afforded by MAS.

The second major complication in the present aluminoborate glass system arises from the fact that both ^{11}B and ^{27}Al are $I > \frac{1}{2}$ nuclei. Due to strong quadrupolar interactions, the various Zeeman transitions are anisotropically broadened and shifted relative to each other. A relatively simple situation arises in the (not uncommon) case $H_Q^{(2)} \ll H_{rf} \ll H_Q^{(1)}$. In this case, the first-order quadrupolar splitting is sufficiently large that the 180° pulses affect only the spin populations contributing to the central $|\frac{1}{2}\rangle \leftrightarrow |-\frac{1}{2}\rangle$ transition, while the line broadening due to the second-order effects is moderately small, such that the central transition is uniformly excited. Provided further that the spin–lattice relaxation times are long on the time scale of the REDOR experiment, only the I nuclei contributing to the central transition produce S spin dephasing. While this situation simplifies the problem conceptually, it is not clear how realistically it can be accomplished in practice. In fact, the recent simulations by Chopin et al. cast severe doubts on the "central level assumption".[47] To facilitate a discussion of the present experimental results, we simply introduce a matrix-element factor f ($0 \leq f \leq 1$) into eq 4,

$$\frac{\Delta S}{S_0} = \frac{4}{3\pi^2}(NT_r)^2 fM_2^{IS} \quad (5)$$

taking into account the reduced probability of I nuclei in the noncentral Zeeman states to contribute to the REDOR dephasing of S spin coherence. In principle, the numerical value of f will be determined by (1) the magnitude of the quadrupolar splitting, (2) the spinning frequency, (3) the radio frequency (rf) field strength, and (4) experimental imperfections such as finite rf pulse lengths, pulse length missets, and phase errors. The results of the present study (see below) indicate that there is very little variation in the ^{11}B and ^{27}Al quadrupolar coupling constants among the different samples. Furthermore, special care was taken to ensure that all of the REDOR results were obtained under identical experimental conditions (rf power and spinning speed). Therefore, it is safe to assume, in each type of REDOR experiment, that f possesses a constant value for all of the samples investigated in the present study. Thus, compositional

trends in the ^{27}Al–^{11}B heterodipolar interaction strength can be analyzed and discussed in terms of the quantity fM_2^{IS}.

2-D Cross-Polarization Heteronuclear Correlation under Magic Angle Spinning. Another double-resonance technique for probing spatial proximity is the CPMAS experiment (Figure 1c). As previously discussed by several authors, the specific challenge for CPMAS involving two different quadrupolar spin systems, I and S, is to realize Hartmann–Hahn matching conditions at rf field strengths (and rotor frequencies) where the central coherences belonging to both spin species remain spin-locked under MAS for several milliseconds.[25,58] Thus, a detailed characterization of the spin-lock behavior of the two quadrupolar spin species is necessary prior to conducting CPMAS experiments. Furthermore, when the MAS spinning frequency exceeds the strength of the homonuclear I–I interactions (commonly known as the "fast spinning limit"), the Hartmann–Hahn matching condition at which an efficient coherence transfer from spins I to spins S could occur is modified to be[55-57]

$$\nu_{1I} - \nu_{1S} = \pm n\nu_r \quad (6)$$

or

$$\nu_{1I} + \nu_{1S} = n\nu_r \quad (7)$$

where ν_1 is the precession frequency of spin $\frac{1}{2}$ nuclei in the applied spin-lock field, ν_r is the MAS rotor frequency, and n takes the integer values of 1 or 2. The first condition (eq 6) corresponds to an energy exchange of two spin species via a spin flip-flop process assisted by mechanical rotation (heteronuclear zero-quantum CP), while eq 7 describes the double-quantum CP analogue (flip-flip or flop-flop). In our previous communication, it has been shown that double-quantum CP is particularly well-suited for quadrupolar nuclei with significant second-order quadrupolar broadening.[48] Taking into account the effective precession frequencies (nutation frequencies),[59,60] the Hartmann–Hahn condition for the double-quantum CP between central transitions of quadrupolar spin systems becomes[48]

$$\nu_{1I}(I + \frac{1}{2}) + \nu_{1S}(S + \frac{1}{2}) = n\nu_r \quad (8)$$

In the present study, these concepts will be applied to aluminoborate glasses for probing ^{11}B $\leftrightarrow$ ^{27}Al dipole–dipole couplings through 2-D heteronuclear correlation (HETCOR) spectroscopy, which can be accomplished by the experiment shown in Figure 1d. Here, the contact period t_c is preceded by chemical shift evolution of the I spin magnetization for an incremented evolution period, t_1. Fourier transformation with respect to the time variables t_1 and t_2 produces a 2-D correlation plot, in which I–S interactions owing to site connectivity or spatial proximity show up as cross-peaks. In addition, variable contact time CPMAS experiments will be reported. Although to date there is no comprehensive theoretical description of the CP dynamics among quadrupolar spin systems, it is the working assumption of this study that the rate of signal buildup at short evolution times is an exponential function of the contact time, reflecting mainly the heterodipolar coupling strengths and the number of

(54) Bertmer, M.; Eckert, H. *Solid State Nucl. Magn. Reson.* **1999**, in press.

(55) Meier, B. H. *Chem. Phys. Lett.* **1992**, *188*, 201.
(56) Stejskal, E. O.; Schaefer, J.; Waugh, J. S. *J. Magn. Reson.* **1977**, *28*, 105.
(57) Marks, D.; Vega, S. *J. Magn. Reson.* **1996**, *118A,* 157.
(58) Sun, W.; Stephen, J. T.; Potter, L. D.; Wu, Y. *J. Magn. Reson.* **1995**, *116A*, 181.
(59) Kentgens, A. P. M.; Lemmens, J. M. M.; Geurts, F. M. M.; Veeman, W. S. *J. Magn. Reson.* **1987**, *71*, 62.
(60) Samoson, A.; Lippmaa, E. *Phys. Rev.* **1983**, *B28*, 6567.

Table 1. Compositions and the Measured T_g Values of the Glasses under Study

	composition, (mol %)					
glass	Na$_2$O	CaO	MgO	B$_2$O$_3$	Al$_2$O$_3$	T_g (°C)
Na-I	20			50	30	484
Ca-I		25		50	25	
Mg-I			25	45	30	665
Na-II	40			40	20	376
Ca-II		40		40	20	
Mg-II			40	40	20	661

Table 2. Hartmann-Hahn Matching Conditions Observed in the ^{11}B{^{27}Al} CPMAS Experiments

glass	ν_R (kHz)	$\nu_{1,B}(I + ^1/_2)$ (kHz)	$\nu_{1,Al}(S + ^1/_2)$ (kHz)	Δ^a (kHz)
Na-I	12	8.9	3.2	0.1
Ca-I	12	7.6	6.2	1.8
Mg-I	12	8.3	6.2	2.5
Na-II	12	7.1	4.6	−0.3
Ca-II	12	8.3	4.2	0.5
Mg-II	12	8.3	8.3	4.6

^{a} This quantity, defined as $\nu_{1,B}(I + ^1/_2) + \nu_{1,Al}(S + ^1/_2) - \nu_R$, indicates the deviation from the double-quantum CP mechanism.

I and S spins involved. Based on this assumption, qualitative trends will be explored for the present series of samples.

Experimental Section

Sample Preparation and Characterization. The glasses under study were prepared by melting the starting materials Na$_2$CO$_3$ (99%, Fluka), MgO (97%, Merck), Al$_2$O$_3$ (99%, Merck), and B$_2$O$_3$ (99%, Merck) separately in platinum crucibles. The melts were then quenched to room temperature by pouring onto a water-cooled copper block. The samples were visually transparent and did not show any sharp X-ray powder diffraction peaks. Weight losses were in close agreement to calculated values, indicating that the chemical compositions of the glasses are close to the batched ones. Glass transition temperatures, T_g, were measured by differential scanning calorimetry (Netzsch DSC 200). Table 1 summarizes the glass compositions and the T_g values obtained.

Solid-State NMR Experiments. Solid-state NMR experiments were carried out on a Bruker DSX-500 spectrometer. At the field strength of 11.74 T, the resonance frequencies are 130.3 and 160.5 MHz for ^{27}Al and ^{11}B, respectively. All the spectra were recorded using a 4-mm Bruker triple-resonance probe. MAS experiments were performed at a rotor frequency of 12 000 ± 2 Hz, at ambient temperature. ^{27}Al SATRAS spectra were obtained under the following conditions: spinning speed, 12 kHz; pulse length, 0.6 μs; recycle delay, 1 s. All the ^{27}Al TQMAS spectra were obtained at a spinning rate of 12 kHz by the z-filtering sequence.[49] The rf field strengths of the first two hard pulses and the third soft pulse corresponded to nutation frequencies of approximately 135 and 6 kHz, respectively, for a liquid sample. The optimized pulse widths were determined to be 3.0, 1.0, and 12.5 μs for the three consecutive pulses. A 72-step phase cycle was employed to select the TQ coherences and cancel all transverse magnetization after the second hard pulse. Typically 576 transients were accumulated for each t_1 increment, and a total of 64 increments were done at steps of 5 μs. A relaxation delay of 0.2 s was employed. Quadrature detection in the F_1 dimension was achieved by the hypercomplex approach. The sheared spectra were analyzed by projecting each individual site onto the F_1 and F_2 axes. Chemical shifts and quadrupolar shifts were obtained according to published procedures.[61]
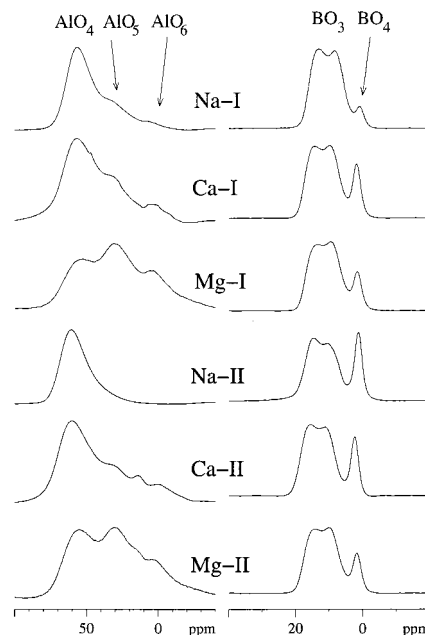
^{11}B{^{27}Al} and ^{27}Al{^{11}B} REDOR studies were carried out using the standard pulse sequence (Figure 1b) with the XY8 phase cycle.[51] To check for artifacts, the experimental conditions were systematically varied (spinning frequencies 6 and 12 kHz). Also, the effect on the S spin dephasing of the rf power level used for applying 180° (I) pulses was tested. Typical power levels corresponded to 180° pulse lengths of 6.0 μs, for both ^{11}B and ^{27}Al.

All CPMAS experiments were recorded in the limit of weak irradiation, conforming to approximate fulfilment of the double-quantum Hartmann–Hahn matching condition (eq 8). This condition was experimentally verified in a ^{11}B{^{23}Na} CPMAS experiment of a polycrystalline sample of Na$_2$B$_4$O$_7$.[48] For the present glasses, it is necessary, however, to make minor empirical adjustments to this condition for optimizing signal enhancement. The nutation behavior was carefully characterized in order to determine the rf field strengths at each Hartmann–Hahn matching condition. Specifically, the Hartmann–Hahn conditions for each set of CPMAS experiments are reported in Table 2. Typically, 2048 transients were accumulated for each CPMAS spectrum. Relaxation delays were 0.2 and 5s for

(61) Fernandez, C.; Amoureux, J. P.; Chezeau, J. M.; Delmotte, L.; Kessler, H. *Microporous Mater.* **1996**, *6*, 33.

Figure 3. ^{27}Al and ^{11}B MAS NMR spectra of all the glasses studied.

^{11}B{^{27}Al} and ^{27}Al{^{11}B} CPMAS, respectively. All of the CP experiments were conducted with spin temperature inversion. In addition, the CP signals were authenticated by routinely conducting null experiments (without pulses on the decoupling channel). Isotropic chemical shifts of ^{27}Al and ^{11}B are reported with respect to 1 M AlCl$_3$ and BF$_3$·Et$_2$O, respectively.

Results and Data Analysis

Single-Resonance NMR. Figure 3 shows the ^{11}B MAS and ^{27}Al MAS spectra of all of the glasses. Note the facile distinction between three- and four-coordinated boron sites. The three-coordinated BO$_{3/2}$ units are dominant and are identified by a structured ^{11}B MAS NMR line shape governed by second-order nuclear electric quadrupolar interactions. In addition, a sharp line is observed attributable to tetrahedrally coordinated boron (BO$_{4/2}$ units). Because of their more symmetric local environment, their ^{11}B resonances are sharp and unaffected by second-order quadrupolar effects. Table 3 summarizes the respective percentages of both types of units, extracted by standard line shape simulation techniques.[43] These simulations also yield chemical shift and quadrupolar coupling parameters, which are summarized in Figure 4. Note that, with the exception of glass Na-I, the percentages of BO$_{4/2}$ units are very similar from sample to sample.

In contrast to the ^{11}B NMR results, Figure 3 reveals striking differences in the ^{27}Al NMR spectra of the glasses: while in the sodium aluminoborate glasses the overwhelming majority of aluminum species are four-coordinated, the calcium and magnesium aluminoborate glasses contain, in addition, substantial fractions of AlO$_5$ and AlO$_6$ units. Their relative proportions

Site Connectivities in Amorphous Materials

J. Am. Chem. Soc., Vol. 121, No. 22, 1999 5243

Table 3. Quantification of Local Structural Units in the Samples Studied[a]

glass	% $BO_{4/2}^-$ ($\pm 10\%$)	% $BO_{3/2}$ ($\pm 10\%$)	% $AlO_{4/2}^-$ ($\pm 5\%$)	% Al^{3+} AlO_5 ($\pm 5\%$)	% Al^{3+} AlO_6 ($\pm 5\%$)
Na-I	2.6	97.4	83	15	2
Ca-I	10.8	89.2	83	11	6
Mg-I	8.0	92.0	49	41	10
Na-II	13.7	86.3	>99		
Ca-II	12.0	88.0	80	11	9
Mg-II	8.9	91.1	61	32	7

[a] The ions Al^{3+} exist as five- or six-coordinated aluminum sites; data for the boron site were corrected according to Massiot's procedure.[63]
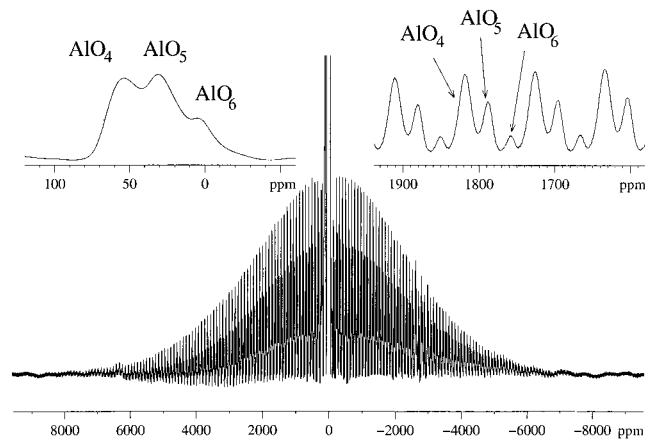
Figure 4. ^{27}Al central and satellite transition spectra of the Mg-II glass. The complete spectrum with the sidebands is shown together with the central resonance (top left) and four selected sidebands (top right) on an expanded scale.
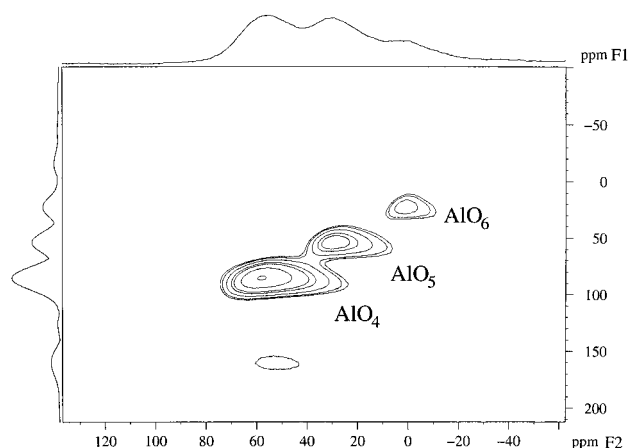
Figure 5. Typical ^{27}Al TQMAS spectrum of the Mg-II glass. Spectroscopic features typical of four-, five-, and six-coordinate aluminum are specifically indicated. Minor peaks are spinning sideband artifacts.

are hard to estimate from the central transition spectra in Figure 3, because the resolution is limited by second-order quadrupolar broadening effects. As mentioned above, however, second-order effects can be suppressed in the ^{27}Al NMR spectra by using either the SATRAS or the TQMAS techniques. Representative data are shown in Figures 4 and 5, demonstrating that the expected resolution improvement can, indeed, be realized in the glassy state. Figure 4 shows a ^{27}Al spinning sideband manifold associated with the $|^1/_2> \leftrightarrow |^3/_2>$ transitions, which is produced by the anisotropy of the first-order quadrupolar interaction. Each individual set of sidebands (inset, top right) shows much superior

Table 4. NMR Parameters for the Glasses Determined by TQMAS and MAS Experiments[a]

| glass	structural units	C_Q (MHz) (± 0.02)	η	χ (MHz) (± 0.02)	δ_{iso} (ppm) (± 1.0)
Na-I[b]	$BO_{3/2}$	2.68	0.23		17.4
	$BO_{4/2}$				0.8
	$AlO_{4/2}$			4.3	63.9
	AlO_5			4.6	37.1
	AlO_6			3.6	8.0
Ca-I	$BO_{3/2}$	2.67	0.35		18.8
	$BO_{4/2}$				1.8
	$AlO_{4/2}$			5.2	64.7
	AlO_5			6.0	43.1
	AlO_6			5.7	10.7
Mg-I	$BO_{3/2}$	2.67	0.38		18.5
	$BO_{4/2}$				1.6
	$AlO_{4/2}$			5.7	65.9
	AlO_5			5.0	37.5
	AlO_6			4.6	8.3
Na-II[b]	$BO_{3/2}$	2.72	0.05		17.8
	$BO_{4/2}$				1.2
	$AlO_{4/2}$			4.3	69.5
	AlO_5			3.9	41.6
	AlO_6			3.1	10.1
Ca-II	$BO_{3/2}$	2.66	0.35		19.7
	$BO_{4/2}$				1.9
	$AlO_{4/2}$			5.1	69.8
	AlO_5			4.4	36.4
	AlO_6			3.0	3.8
Mg-II	$BO_{3/2}$	2.66	0.36		19.1
	$BO_{4/2}$				1.7
	$AlO_{4/2}$			5.7	68.1
	AlO_5			4.8	38.5
	AlO_6			3.8	6.3

[a] The ^{27}Al and ^{11}B NMR parameters were determined by TQMAS and MAS experiments, respectively. The quadrupolar coupling of the $BO_{4/2}$ site is weak ($\chi \approx 500-700$ kHz). [b] Data taken from ref 43.

resolution to the central transition spectra (inset, top left), allowing reliable estimates of $AlO_{4/2}$, AlO_5, and AlO_6 concentrations to be obtained. The aluminum speciation deduced in this fashion is included in Table 3. Figure 5 shows a representative result from ^{27}Al TQMAS spectroscopy. In this two-dimensional plot, the regular MAS spectrum along the F_2 dimension is correlated with an isotropic dimension along F_1, in which the resolution is markedly improved owing to the elimination of second-order quadrupolar effects. From the locations of the cross-peaks, values of isotropic chemical shifts and the quadrupolar parameters can be determined; these values are summarized in Table 4 and should be considered averages.[43] The question of how these various types of units are linked to boron is addressed in the double-resonance studies discussed below.

Rotational Echo Double Resonance. Dipolar couplings between the various types of boron and aluminum sites were probed by ^{27}Al\{^{11}B\} and ^{11}B\{^{27}Al\} REDOR experiments for all of the six glasses studied. The results are summarized in Figures 6 and 7, respectively, where the MAS echo difference signal $\Delta S/S_o$ is plotted as a function of dipolar evolution time NT_r. The ^{27}Al\{^{11}B\} experimental results are shown in Figure 6. The curves displayed there were found to be fairly independent of the experimental conditions (spinning speed, rf field strength) used. Furthermore, no significant differences were found between the ^{11}B dipolar field strengths at the three types of aluminum sites (data not shown). This result shows that $AlO_{4/2}$, AlO_5, and AlO_6 units are all well-integrated into the glass structure and do not form phase-segregated regions of aluminum oxide.

To extract more quantitative information on the strength of the ^{11}B$-^{27}$Al dipole$-$dipole couplings, the approximate eq 5

(a)

(b)
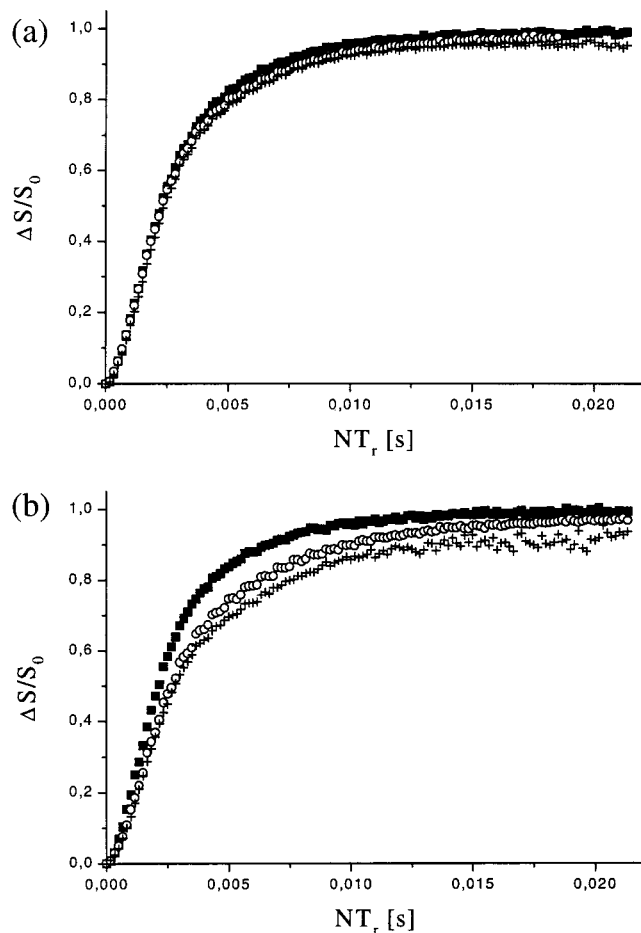
Figure 6. ^{27}Al{^{11}B} REDOR curves of (a) glass I series and (b) glass II series: Mg (■), Ca (○), and Na (+). No spinning speed influence was noted.

was used to extract fM_2 (^{27}Al{^{11}B}) values from the REDOR curves of Figure 6. The data range chosen was $0 \leq \Delta S/S_o \leq 0.2$, because in this limit the dephasing curves are independent of any assumptions made about the spin geometry present (see the simulations of Figure 2). Fitting the short-time behavior of Figure 6 to eq 5 yielded the fM_2 (^{27}Al{^{11}B}) values compiled in the first column of Table 5. These values are all fairly similar, indicating that the local magnetic fields created by the ^{11}B spins at the ^{27}Al nuclear sites are of comparable magnitude in all of the samples studied. This result suggests that the average environment of the aluminum atoms by boron species is rather uniform and affected little by the basic glass composition or the cation type.

The results of the ^{11}B{^{27}Al} REDOR experiments are substantially more complicated, showing a nonnegligible influence of both spinning frequency (see Table 5) and rf power level (not shown) on the steepness of the curves, and thence on the fM_2 (^{11}B{^{27}Al}) values obtained. Thus, care was taken to compare only REDOR data sets obtained under strictly identical experimental conditions. Since Figure 3 reveals that the resonances due to BO$_{3/2}$ and BO$_{4/2}$ units are well-resolved in the ^{11}B MAS NMR spectra, it was possible to obtain separate ^{11}B{^{27}Al} REDOR curves for both boron types; the data are represented by filled and open circles, respectively, in Figure 7. Examination of the different parts of Figure 7 reveals that, in each of the Na and Ca glasses, the ^{11}BO$_{3/2}${^{27}Al} REDOR curves are always steeper than the ^{11}BO$_{4/2}${^{27}Al} REDOR curves. This effect is also clearly evident in the fM_2 values extracted from the initial decays using eq 5, as described above

(again, the data range $0 \leq \Delta S/S_o \leq 0.2$ was used). These values (Table 5, second and third columns) show that the BO$_{3/2}$ sites interact much more strongly with ^{27}Al than the BO$_{4/2}$ sites do. Other results not shown here indicate that this is consistently true for glasses within the entire compositional region of the sodium aluminoborate system. In contrast, the results for the Mg glasses (Figure 7, top) indicate that both the BO$_{4/2}$ and BO$_{3/2}$ sites interact about equally strongly with ^{27}Al nuclei, and the corresponding fM_2 values are found to be identical within experimental error. To address the question of whether this effect is related to the presence of large amounts of AlO$_5$ and/or AlO$_6$ units (Figure 4), 2-D CPMAS−HETCOR experiments were carried out.

Cross-Polarization and Spin-Locking Behavior. Table 2 summarizes the Hartmann−Hahn matching conditions optimized empirically for maximum signal enhancement in the crosspolarization experiments. It is interesting to find that the higher the AlO$_5$ and AlO$_6$ content, the larger the deviation of the empirical Hartmann−Hahn matching (HH) from that of the double-quantum CP (eq 8). Meier shows that, under magic angle spinning, the HH sidebands of the double-quantum and zero-quantum CP are of opposite signs and may partially overlap under the condition $\nu_{1S} - \nu_{1I} < -2\nu_R$.[55] Therefore, the position of the resultant HH sideband maximum depends on the extent of the sideband overlap and could deviate substantially from the matching condition of pure double-quantum or zero-quantum CP. Although a formal theory for the cross-polarization between quadrupolar nuclei is not yet available, it seems that a distribution in quadrupolar coupling constant will increase the widths of the HH sidebands and complicate the resultant position of the sideband maxima.

Figure 8 shows the spin-locking behavior observed for sample Mg-II using the above-specified CP conditions. The relaxation characteristics observed here are typical for all of the samples studied: (1) both the ^{11}B and ^{27}Al spin-locked magnetizations decay nonexponentially; (2) under the chosen conditions, ^{11}BO$_{4/2}$ magnetization decays faster than ^{11}BO$_{3/2}$ magnetization; and (3) within experimental error, AlO$_{4/2}$, AlO$_5$, and AlO$_6$ units have identical rotating frame relaxation behavior. This latter result is important for the interpretation of the HETCOR and semiselective CPMAS data to be presented below.

2-D Heteronuclear Correlation Experiments. A typical 2-D HETCOR spectrum obtained via CPMAS is shown in Figure 9 for the sample Na-I. For all of the glasses, the results reveal the presence of magnetization transfer and hence spatial proximity of boron and aluminum among all possible combinations of the various sites present. However, important differences become apparent from a closer inspection of the cross-peaks. In Figure 9, the ^{27}Al projection from the BO$_{3/2}$ cross-peak closely resembles the regular 1-D MAS NMR spectrum, whereas the ^{27}Al projection from the BO$_{4/2}$ cross-peak shows much larger proportions from five- and six-coordinated aluminum (on a relative basis) than present in the single-pulse ^{27}Al NMR spectrum (Figure 3). Since Figure 8 confirms that this effect cannot arise from differences in ^{27}Al spin-lock behavior (see discussion above), these HETCOR data reveal a preference of the BO$_{4/2}$ units in Na-I to interact with AlO$_5$ and AlO$_6$ sites. A similar tendency was noted in glasses Mg-I and Ca-I, but not in glasses Na-II, Ca-II, and Mg-II (data not shown).

Semiselective Variable Contact Time Experiments. A second approach for imparting some site distinction on CP experiments takes advantage of the fact that, at the low rf powers used, the efficiency of spin-locking becomes greatly dependent on resonance offset effects.[48,58] In particular, Figure 10 shows
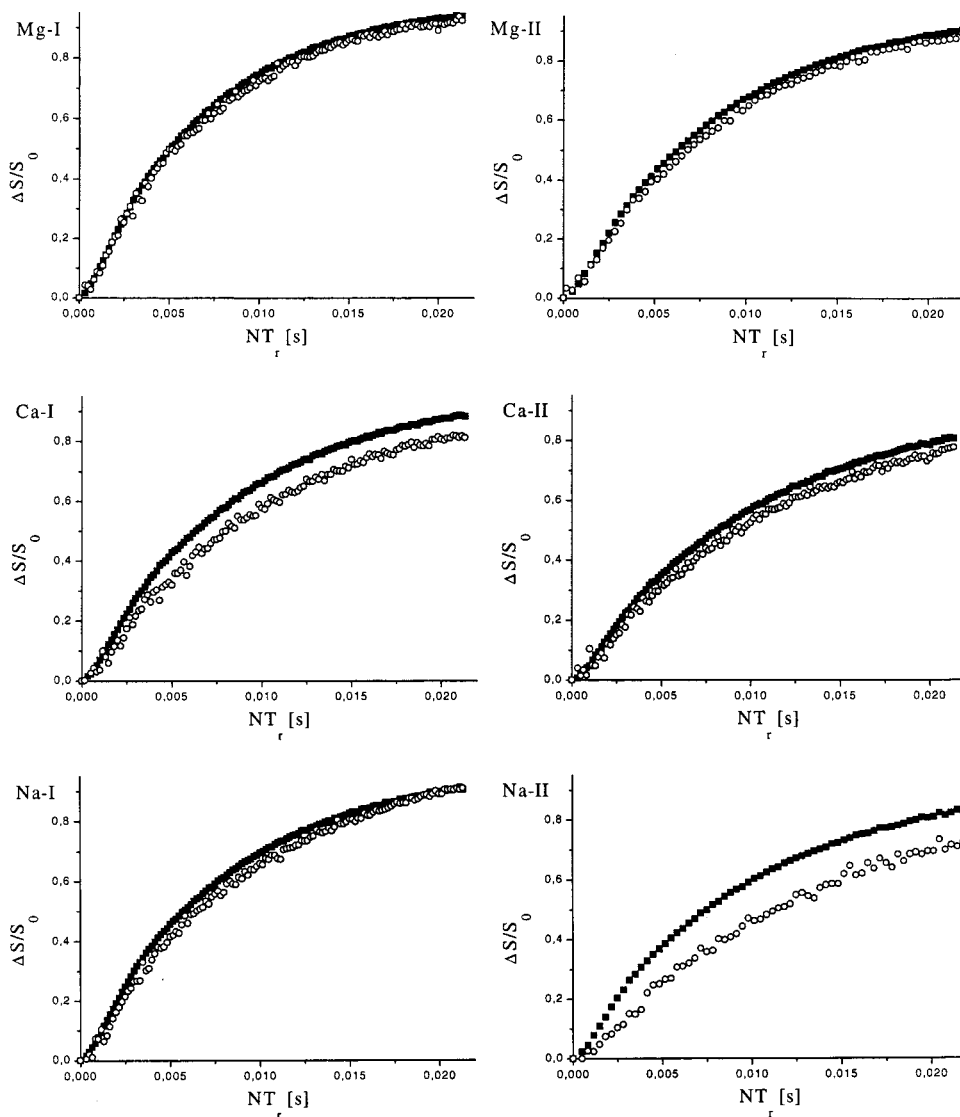
Figure 7. $^{11}B\{^{27}Al\}$ REDOR curves at a spinning speed of 12 kHz: $BO_{3/2}$ (■) and $BO_{4/2}$ (○).

Table 5. Apparent Second Moments (fM_2^{BA1}) Characterizing the Heterodipolar Interaction Strengths of Al⋯B Connectivities Determined from the $^{27}Al\{^{11}B\}$ and the $^{11}B\{^{27}Al\}$ REDOR Experiments

	fM_2^{BA1} ($\times 10^6$ s^{-2})				
glass	^{27}Al-$\{^{11}$B$\}^a$ (±0.1)	^{11}BO$_3$-$\{^{27}$Al$\}^b$ (±0.05)	^{11}BO$_4$-$\{^{27}$Al$\}^b$ (±0.05)	^{11}BO$_3$-$\{^{27}$Al$\}^c$ (±0.05)	^{11}BO$_4$-$\{^{27}$Al$\}^c$ (±0.05)
Na-I	1.2	0.58	0.28	0.40	0.29
Ca-I	1.4	0.52	0.31	0.34	0.22
Mg-I	1.4	0.58	0.59	0.44	0.42
Na-II	1.0	0.42	0.22	0.27	0.09
Ca-II	1.1	0.37	0.20	0.24	0.17
Mg-II	1.6	0.32	0.32	0.26	0.24

^{a} Data are independent of spinning speed. ^{b} Data obtained at a spinning speed of 6 kHz. ^{c} Data obtained at a spinning speed of 12 kHz.

the $^{27}Al\{^{11}B\}$ CPMAS spectra of Mg-I glass at different ^{27}Al resonance offsets. While locating the carrier at the resonance frequency of the central AlO$_5$ peak still produces a fairly representative spectrum, larger offsets lead to substantial deterioration of the signal. As Figure 10 illustrates, the magnetization belonging to the AlO$_{4/2}$ sites cannot be spin-locked effectively if the ^{27}Al carrier is placed at the AlO$_6$ resonance offset and

vice versa (a similar but less dramatic effect is also observed for the ^{11}B carrier frequency, data not shown). Thus, it is possible to obtain ^{11}B spectra via CP from selected aluminum sites. This effect offers novel spectral editing opportunities which were applied to variable contact time experiments. Figures 11 and 12 show the semiselective $^{11}B\{^{27}AlO_4,AlO_5\}$ and $^{11}B\{^{27}AlO_5,AlO_6\}$ CP signal intensities as a function of the contact time, where the ^{27}Al carrier was located at the spectral positions of AlO$_4$ and AlO$_6$, respectively. Each signal buildup curve was normalized internally and approximated by an exponential function at short contact times.[48] As documented by the approximately linear behavior in these semilogarithmic plots of $\ln(1 - M/M_{max})$ vs contact time, crude estimates of the cross-relaxation rate constant $(T_{cp})^{-1}$ can be obtained in this fashion. It is clear that the signal buildup curves are more complicated functions of the spatial proximity, resonance offset, Hartmann–Hahn matching offset, quadrupolar coupling effects, and relaxation behavior in the rotating frame of both types of nuclei involved. Without a theoretical framework to consider these physical factors explicitly, quantitative interpretations of these curves are not warranted. Nevertheless, as discussed above, Figure 8 reveals that the various ^{27}Al coordination sites show more or less identical rotating frame relaxation behavior; this
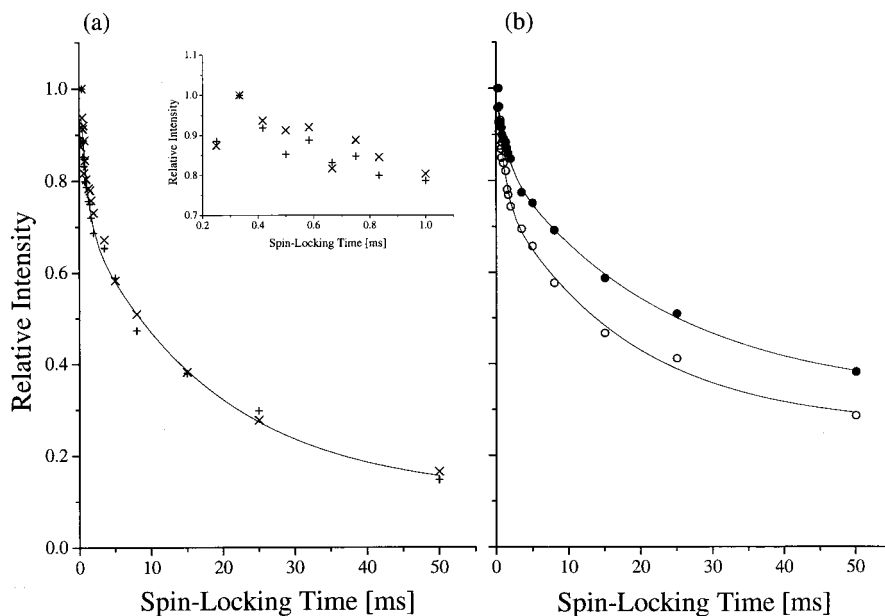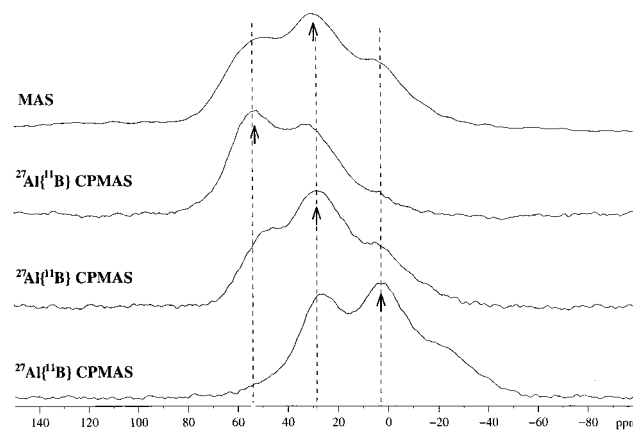
Figure 8. Representative spin-locking results of Mg-II glass. (a) ^{27}Al: +, $AlO_{4/2}$; ×, AlO_6; inset shows the initial behaviors of the two sites. (b) ^{11}B: ●, $BO_{3/2}$; ○, $BO_{4/2}$.
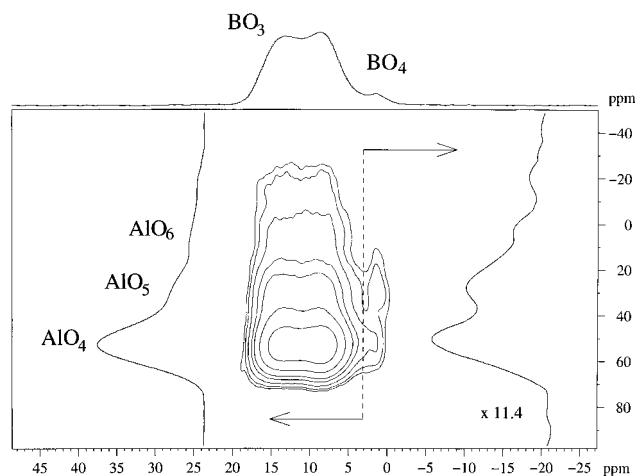
Figure 9. $^{11}B\{^{27}Al\}$ CPMAS−HETCOR spectrum of Na-I glass, including separate ^{27}Al projections from the BO_3 and $BO_{4/2}$ subspectra. A CP contact time of 1.5 ms was used. The F_1 projections of $BO_{4/2}$ are magnified for comparison.

Figure 10. $^{27}Al\{^{11}B\}$ CPMAS spectra of Mg-I glass at different ^{27}Al carrier frequency offsets. The bold arrows indicate the positions of the carrier frequency. Note the semiselective detection of ^{27}Al resonances produced by the off-resonance effect.

was found to be the case for all of the samples studied. For a given sample, it is therefore still reasonable to compare the T_{cp}^{-1} values of the $^{11}BO_{3/2}\{AlO_{4/2},AlO_5\}$ and $^{11}BO_{3/2}\{AlO_5,AlO_6\}$ CPMAS experiments with each other. Likewise, it is possible to compare the corresponding T_{cp}^{-1} values for the $BO_{4/2}$ units of a given sample. These comparisons are documented in Figures 11 and 12 for all of the glasses studied. The T_{cp}^{-1} estimates obtained from the slopes of these plots are listed in Table 6. Slope differences within each figure indicate some degree of interaction selectivity, the steeper slope being associated with the stronger interaction. To facilitate the subsequent discussion, Table 6 lists rate ratios $R = T_{cp}^{-1}(AlO_4,AlO_5)/T_{cp}^{-1}(AlO_5,AlO_6)$ for each type of boron unit. Since all of the other factors are kept identical, the rate ratios mostly reflect preferences in spatial proximity. Inspection of this table reveals that, particularly in glasses Na-I, Ca-I, and Mg-I, R lies substantially below unity for the $BO_{4/2}$ units, suggesting a preferential interaction with AlO_5 and AlO_6 sites. We note that, in contrast, no clear tendency is observed for the glasses Na-II,

Ca-II, Mg-II. This finding is in full agreement with the HETCOR results, confirming in particular the importance of the chemical composition effects noted above. It is clear that, owing to the underlying assumptions made in the present analysis, the T_{cp}^{-1} values listed in Table 6 should be treated with great caution, and no further conclusions should be drawn from those values. In particular, sample-to-sample cross-comparisons are not warranted, because each sample possesses unique rotating frame relaxation rates. Furthermore, the comparisons of $T_{cp}^{-1}(BO_{3/2})$ versus $T_{cp}^{-1}(BO_{4/2})$ estimates are also not legitimate because the rotating frame relaxation curves of the two boron sites are quite different (Figure 8).

Discussion

Based on the detailed results presented above, it is now possible to develop network connectivity models and discuss the pronounced cation effects observed in these glasses. In this connection, the influence of the elemental glass composition must be kept in mind. Detailed previous work has shown that a particularly important parameter influencing the local structure
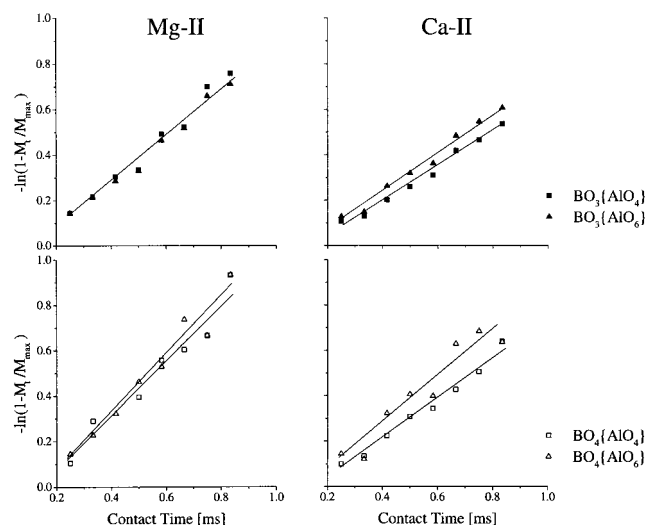
Figure 11. $^{11}B\{^{27}Al\}$ variable contact time experiments of glass series II at different ^{27}Al carrier frequency offsets, corresponding to the ^{27}Al peak locations indicated.

of aluminoborate glasses is the $M_{(2)}O$-to-Al_2O_3 ratio. This ratio is near or below unity for Na-I, Ca-I and Mg-I; the compositions chosen are near the glass-forming borders for all three systems studied. In contrast, $M_{(2)}O/Al_2O_3 = 2.0$ for glasses Na-II, Ca-II, and Mg-II, which is much closer to the centers of the respective glass-forming regions. Thus, the trends observed within the second series might be considered more representative in terms of the principles governing local and *intermediate-range* ordering in most aluminoborate glasses.

Sodium Aluminoborate Glasses. The situation in Na-II is rather simple. As documented by Figure 3, the network structure is dominated by trigonal $BO_{3/2}$ and tetrahedral $AlO_{4/2}$ units. The $^{27}Al\{^{11}B\}$ REDOR data (Figure 6) and the CPMAS−HETCOR data (not shown) reveal that these units are strongly linked, thus ruling out possible scenarios based on chemical segregation or phase separation. In addition, the $^{11}B\{^{27}Al\}$ REDOR experiments (Figure 7, bottom) indicate that the $BO_{4/2}$ units are very remote from tetrahedral aluminum sites, suggesting that they are mostly linked to $BO_{3/2}$ groups. The apparent absence of such intertetrahedral links can be rationalized on the basis of bond valence arguments.[42] Both the $BO_{4/2}$ and $AlO_{4/2}$ sites carry formal negative charges which repel each other. The same principle is known to govern connectivity in silicate and zeolite chemistry (Löwenstein rule).[62] Additional experiments (to be published separately) indicate that this rule is applicable for most of the glasses within the $Na_2O−B_2O_3−Al_2O_3$ glass-forming region. An interesting additional effect occurs for glass Na-I, whose composition is close to the glass-forming border. Since the Na_2O/Al_2O_3 ratio is below unity, a substantial fraction of more highly coordinated aluminum is predicted−and found experimentally by ^{27}Al NMR (Table 3, Figure 3). Furthermore, a comparison of the $^{11}B\{^{27}Al\}$ REDOR curves (Figure 7, bottom left vs bottom right) indicates that the $BO_{4/2}$ units in the Na-I glass show a much stronger interaction with aluminum than those in the Na-II glass. This effect is easily understood on the basis of the 2-D HETCOR and the semiselective CPMAS data reported here: both experiments consistently reveal a particularly favorable interaction between $BO_{4/2}$ units and more highly coordinated aluminum (see Figure 9 and Table 6). This finding is in excellent agreement with the bond valence predictions by

Brow and co-workers, and to our knowledge the present study provides the first experimental evidence for this effect.

Calcium Aluminoborate Glasses. Table 3 and Figure 3 reveal that, in Ca-I and Ca-II, the structural speciation of aluminum clearly differs from that in Na-II but appears to be quite similar to that in Na-I. Although the large majority of aluminum is present as $AlO_{4/2}$ sites, these glasses contain also significant fractions of more highly coordinated aluminum, in agreement with previous findings.[40] The $^{11}B\{^{27}Al\}$ REDOR data (Figure 7, middle) indicate strong $^{11}B−^{27}Al$ interactions in the network, although there is a clear difference between the $BO_{3/2}$ and the $BO_{4/2}$ units. The HETCOR results (not shown) and the semiselective CPMAS results (Figures 11 and 12) reveal further that, in Ca-I, the $BO_{4/2}$ sites interact more favorably with the more highly coordinated aluminum units than with the dominant $AlO_{4/2}$ sites; the effect is much less pronounced in Ca-II. Overall, the results indicate that, as in the sodium-based glasses, the intermediate-range order of these glasses is characterized by at least partial avoidance of intertetrahedral links.

Magnesium Aluminoborate Glasses. The behavior observed for Mg-I and Mg-II is distinctly different from that seen in the Na- or Ca-bearing glasses with comparable compositions: the fractions of AlO_5 and AlO_6 units are significantly increased (Figures 3−5), and the $BO_{4/2}$ units interact much more strongly with aluminum than they do in the other glasses (Figure 7, top). As a matter of fact, the $^{11}B\{^{27}Al\}$ REDOR curves show no more distinction between $BO_{3/2}$ and $BO_{4/2}$ units in this experiment (Table 5). For Mg-I, the CPMAS results (Tables 5 and 6) suggest that the $BO_{4/2}$ units are preferentially surrounded by AlO_5 and/or AlO_6 groups. To the contrary, no significant connectivity preferences are detected in Mg-II. These results indicate that Löwenstein's avoidance rule is not obeyed in the latter glass, and a structure governed by statistical linking seems the most appropriate description.

Composition and Cation Effects. Overall, the experimental trends discussed above reveal pronounced effects of both composition and cation type. These trends are summarized schematically in Figure 13. The cation effect is most clearly seen within the series II glasses. As Na^+ is replaced by Ca^{2+} and further by Mg^{2+}, the aluminum speciation becomes more diverse, and the site connectivity principle changes from strong chemical ordering to statistical. These effects can be easily understood in terms of the cation's polarizing strength, which increases in the order $Na^+ \rightarrow Ca^{2+} \rightarrow Mg^{2+}$. In glasses with weakly polarizing cations, chemical ordering such as the avoidance of intertetrahedral links are clearly important; hence, bond valence models can be used in predicting stable local connectivities. In contrast, in glasses with high field strength cations such as Mg^{2+}, these local energy terms become much less important, resulting in randomization. This competition and interplay of both enthalpy and entropy factors is further highly dependent on compositional parameters such as the $M_{(2)}O/Al_2O_3$ ratio: glasses of series I give strong evidence for a chemical preference of $BO_{4/2}$ units to interact with more highly coordinated aluminum sites; this is not observed for series II glasses.

Conclusions

While the presence of ^{11}B and ^{27}Al quadrupolar splittings complicates the execution and interpretation of both REDOR and CPMAS experiments considerably, an appropriate strategy has been designed to retrieve remarkable detail on the structures of aluminoborate glasses. While advanced high-resolution solid-state NMR measurements help in estimating the various types of local environments present, the connectivities of these sites

(62) Loewenstein, W. *Am. Miner*. **1954**, *39*, 92.
(63) Massiot, D.; Bessada, C.; Coutures, J. P.; Taulelle, F. *J. Magn. Reson.* **1990**, *90*, 231.
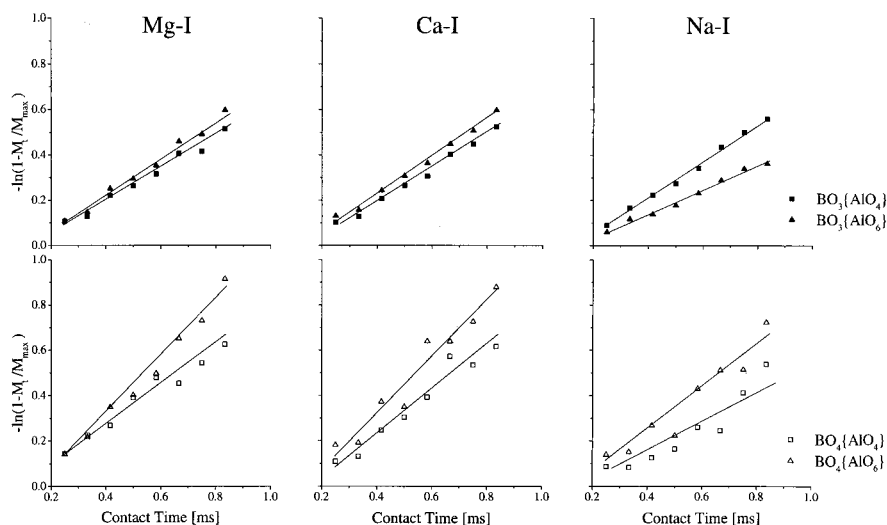
Figure 12. ^{11}B$\{^{27}$Al$\}$ variable contact time experiments of glass series I at different ^{27}Al carrier frequency offsets corresponding to the ^{27}Al peak locations indicated. Data for Na-II are not shown because the amount of AlO$_6$ units is negligible in this glass.

Table 6. Cross-Relaxation Rates ($1/T_{cp}$) between Boron and Aluminum Sites of Glasses under Study[a]

| glass	BO$_3\{$AlO$_4\}$ (ms^{-1})	BO$_3\{$AlO$_6\}$ (ms^{-1})	R	BO$_4\{$AlO$_4\}$ (ms^{-1})	BO$_4\{$AlO$_6\}$ (ms^{-1})	R
Na-I	0.81(2)	0.53(2)	1.5	0.75(11)	0.98(12)	0.76
Ca-I	0.74(3)	0.81(3)	0.91	0.95(8)	1.24(11)	0.77
Mg-I	0.70(4)	0.83(4)	0.84	0.80(6)	1.28(7)	0.63
Ca-II	0.77(4)	0.86(4)	0.90	0.90(5)	1.02(13)	0.88
Mg-II	1.07(7)	1.00(6)	1.1	1.24(12)	1.29(11)	0.96

[a] Data for glass Na-II are not given since the amount of AlO$_6$ is negligible in this glass; hence, R cannot be calculated.

are probed effectively by REDOR and CPMAS/HETCOR experiments.

Application of this strategy to the present series of glasses indicates that the structural speciation and connectivity landscape of aluminoborate glasses is controlled by both the glass composition and the ionic field strength of the alkali or alkaline-earth cation present. For the Na- and Ca-bearing glasses, the REDOR results indicate that intertetrahedral links are largely avoided. This finding constitutes a remarkable degree of *intermediate-range order*. In contrast, magnesium-containing glasses are characterized by a randomization of connectivities. Detailed ^{11}B$\{^{27}$Al$\}$ CPMAS experiments indicate further that, at certain glass compositions (series I), the tetrahedral units have a tendency to interact preferentially with more highly coordinated aluminum (AlO$_5$ and/or AlO$_6$ sites). While the present study mostly addresses the methodology, future work will be concerned with the detailed dependence of these results on the chemical compositions of these glasses.

The remaining challenge for a complete description of the *intermediate-range order* in aluminoborate glasses is a similarly structured investigation of the homonuclear correlations among
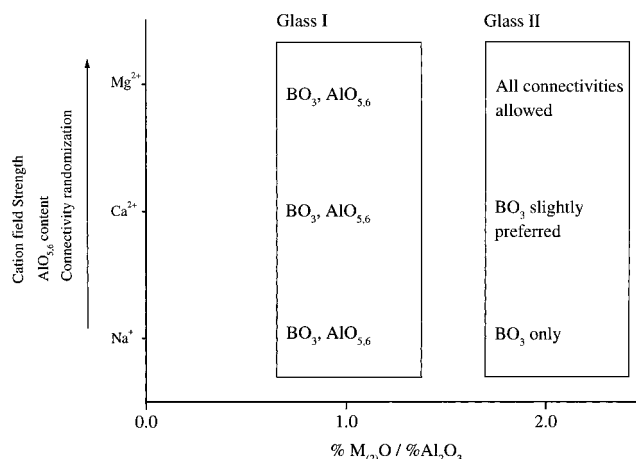
Figure 13. Structural trends in aluminoborate glasses as a function of M$_{(2)}$O/Al$_2$O$_3$ ratio and cation type. Preferred connectivities for the tetrahedral BO$_{4/2}$ and AlO$_{4/2}$ units are indicated.

the various types of aluminum sites and among the respective boron sites. For spin $^1/_2$ nuclei, this task can be accomplished with the help of double-quantum MAS NMR spectroscopy. Transfer of this approach to quadrupolar nuclei is currently under investigation in our laboratory.